Effects of chamber geometry, hydrogen ratio and EGR ratio on the combustion process and knocking characters of a HCNG engine at the stoichiometric condition

Bin Liang [a], Lei Cheng [b], Meng Zhang [a], Yongcheng Huang [a], Jinhua Wang [a], Yongzheng Liu [c], Fanhua Ma [c], Zuohua Huang [a],[*]

[a] *State Key Laboratory of Multiphase Flow in Power Engineering, Xi'an Jiaotong University, Xi'an 710049, China*
[b] *Pipe China Institute of Science and Technology, Lang fang 065000, China*
[c] *State Key Laboratory of Automotive Safety and Energy, Tsinghua University, Beijing 100084, China*

ARTICLE INFO

ABSTRACT

Stoichiometric operation natural gas engine can achieve low emissions and high-power output by combining EGR and three-way catalytic converter. However, under high load conditions, engine performance will be deteriorated due to the knocking limits. The main methods to solve the knocking problems of spark ignition engines are shortening the flame propagation time and reducing the temperature and pressure rise of the end mixture. This paper firstly established a 3D model based on a natural gas engine, and then conducted the numerical simulations to investigate the effects of chamber geometry, hydrogen ratio and EGR ratio on engine knocking and combustion. The validation indicates a satisfied numerical results of chamber pressure and heat release rate. The turbine chamber exhibits relatively better swirl and tumble, thus achieving the highest turbulence intensity. HCNG fuel will increase the knocking tendency of the engine. In the meantime, the addition of hydrogen will also reduce the IMEP of the engine due to the low volume heat value of hydrogen. However, the addition of hydrogen may accelerate the combustion rate at the end of combustion to a certain extent. EGR can significantly reduce the knocking tendency of HCNG engine by reducing the combustion temperature in the cylinder. Compared with the case of 14% EGR rate, the ignition angle of 30% EGR case is advanced by 19 °CA, and the indicated thermal efficiency is increased by 2.06%.

Introduction

Compressed natural gas (CNG) has great application potential in the automotive industry, especially in the field of heavy commercial vehicles, due to its low cost, high H/C ratio and high-octane number [1]. To meet the increasingly stringent emission regulations, the lean burn limit of natural gas engines still needs to be expanded. However, combustion deterioration and thermal efficiency reduction will occur near the engine operation limits. Stoichiometric operation natural gas engine can achieve low emissions and high-power output by applying exhausted gas recirculation (EGR) combined with three-way catalytic converter [2]. Natural gas has the characteristics of relatively slow flame speed and long combustion duration. For heavy commercial vehicles, the engine is usually operated at full load during the acceleration process, resulting in severe knocking which limits the engine performance. Therefore,

improving the knocking boundary becomes the key topic of stoichiometric operation natural gas engine. At present, this is solved by shortening the flame propagation time and reducing the temperature and pressure of the end mixture in spark ignition engines.

Increasing turbulence intensity in combustion chamber is an effective way to accelerate flame propagation and improve combustion performance. The mean velocity and turbulence intensity of the flow field determine the development of the initial flame core. The subsequent flame propagation has been considered to be mainly affected by the heat and mass transfer of large-scale and small-scale turbulence. In addition, the flow field in the chamber is largely decided by the chamber geometry. Therefore, combustion chamber geometry can significantly affect the knocking and combustion characteristics of CNG engines. The investigations conducted by Lund University of Technology [3,4] studied 10 different piston geometries and found that the combustion characteristics were significantly different, among which the cylindrical

Nomenclature			
κ	mean flame front curvature	CA90	crank angle for 90% of the heat release
ρ_u	unburned gas density	CEQ	chemical equilibrium
ω	angular speed	CNG	compressed natural gas
a_4, b_1, b_3	model constants	EGR	exhausted gas recirculation
D_a	the Damköhler number	HCNG	hydrogen enriched compressed natural gas
D_t	turbulent diffusion term	IMEP	indicated mean effective pressure
S_l	laminar flame speed	ITE	indicated thermal efficiency
S_t	turbulent flame speed	KI	knocking intensity
u'	turbulence speed fluctuation	PPmax	maximum peak value of pressure oscillation
3-D	three-dimensional	TKE	turbulent kinetic energy
AMR	adaptive mesh refinement	TR	tumble ratio
ATDC	after top dead center	RANS	Reynolds-averaged Navier–Stokes
CA	crank angle	RNG	renormalization group
CA10	crank angle for 10% of the heat release	RON	research octane number
CA50	crank angle for 50% of the heat release	SR	swirl ratio
		TLF	tabulated laminar flame-speed

and square piston top shapes provided the highest turbulence. In the main part of combustion, there was a high correlation between in-cylinder turbulence and heat release rate, and the combustion duration was more affected by the average speed and turbulence. Li et al. [5] studied the effect of six different combustion chamber structures on turbulence intensity for natural gas engines. They found that hexagonal geometry had the best enhancement effect on turbulence intensity. The following literature [6] has also done relevant research. However, piston with hexagon and square shapes are relatively special, which are seldomly used in the practical engines due to its sharp angles. At present, the top surface of combustion chamber piston used in natural gas engines is mostly based on cylindrical structure. Yan et al. [7] studied the effect of the reentrant size of the combustion chamber on knocking and combustion in a stoichiometric operation natural gas engine. The results showed that with the reduction of the diameter ratio, the combustion duration could be continuously shortened, which was beneficial to improve the engine thermal efficiency. However, engine was tended to increase knocking tendency and heat loss in the meantime. Zhao et al. [8] studied the effects of different combustion chamber structures on knocking and combustion based on LNG engines. The results showed that improving the turbulent kinetic energy (TKE) in the combustion chamber could effectively promote flame propagation. Proper turbulent kinetic energy distribution was beneficial to shorten the combustion duration and obtain good anti-knocking performance. Zhu et al. [9] studied the impact of intake manifold coupling with different piston top surfaces on knocking and combustion of natural gas engines and found that the combination of spiral intake manifold and turbine chamber showed better anti-knocking performance.

In recent years, clean alternative energy has been increasingly concerned worldwide. Among all these potential fuels, hydrogen is considered to be the most desirable alternative fuel. Hydrogen can be obtained from electrolysis of water and the electricity used can be generated by solar energy, which indicates that hydrogen is a kind of future promising renewable energy. At the same time, the physical and chemical properties of hydrogen are different from those of traditional fossil fuels. Firstly, as a carbon free fuel, hydrogen does not produce carbon dioxide during the combustion process. Secondly, compared with natural gas, hydrogen has faster flame propagation speed and higher-octane number, which is more conducive to improving thermal efficiency. Therefore, hydrogen enriched compressed natural gas (HCNG) fuel can significantly improve the problems of long combustion duration and high emissions of CNG. Ma et al. of Tsinghua University [10,11] studied the combustion and emission characteristics of HCNG engine under different hydrogen ratios, loads, ignition angles and equivalence ratios. Bartosz et al. [12] have done similar work. Sagar

et al. [13] studied the knocking and emission characteristics under different hydrogen ratios and found that HCNG significantly reduced carbon emissions, but increased nitrogen oxide emissions. At the same time, the knocking intensity of 30% HCNG fuel was the lowest.

The addition of hydrogen increases the combustion temperature in the cylinder, which will aggravate the occurrence of knocking to a certain extent. EGR can significantly reduce the temperature in the cylinder, thus reducing the tendency of knocking and improving the thermal efficiency of the engine. Yu et al. [14] used EGR to expand the output limit of kerosene engine under the knocking limit. The results showed that when the EGR rate increased from 0% to 10%, the indicated mean effective pressure (IMEP) at the knocking limit increased by 7% due to the increase of the intake volume. At the same time, because of the high specific heat ratio and reduced heat loss, the specific fuel consumption was reduced by 8.1%, and the indicated thermal efficiency (ITE) was increased from 23.5% to 25.6%. Zhen and Wang et al. of Tianjin University [15,16] studied the effect of EGR rate on engine knocking suppression for methanol fuel. The results showed that EGR could reduce the knocking intensity and delay the knocking start time. Meanwhile, with the increase of EGR rate, the thermal efficiency was greatly reduced. Wei et al. [17] studied the knocking characteristics of n-butanol and RON 92 gasoline, and compared the knocking initiation time, intensity and frequency at different EGR rates. The results showed that EGR could reduce the knocking intensity and delay the knocking start time due to its cooling and dilution effects. It was observed that at a low EGR rate of 3%, the knocking intensity of n-butanol decreased significantly. Similar studies have been carried out in literature [18,19].

Overall, the reasonable combustion chamber geometry will increase the turbulence intensity of the engine and accelerate the flame propagation speed. The addition of hydrogen increases the flame propagation speed and combustion chamber temperature, which increases the knocking tendency. However, increasing EGR can suppress knocking by reducing the combustion chamber temperature, but it also reduces fuel suplement and worsens IMEP. The combination of HCNG and EGR has a complicated effect on the knocking. Although numerous studies have been conducted on the combustion characteristics of the HCNG engine, the comparative laws of knocking and combustion are still not clear. In addition, most of the studies are only aimed at the combustion and emission characteristics of the HCNG engine, and the simulation of knocking and combustion is relatively lacking. A great deal of research has been devoted to the effect of EGR on the knocking and combustion of methanol and gasoline engines, while there is still a lack of research on the stoichiometric operation HCNG engines. Therefore, the influence of different combustion chamber structures on knocking and combustion of natural gas engine was studied by numerical simulation method. Then

the effects of different hydrogen ratios and EGR ratios on knocking and combustion of stoichiometric operation natural gas engine were studied with the best combustion chamber structure.

Methodologies

Experimental setup

Figure 1 shows the engine test platform used in this study. HCNG internal combustion engine is connected with the eddy current dynamometer through the adapter shaft. By controlling the throttle opening and engine speed, the engine can be operated within full loads. The working performance could be monitored by the German HBM high-precision torque sensor (sensitivity: ±0.05%). The HORIBA-MEXA-7100DEGR emission monitoring system was used to measure NOx, THC, CO, and CH_4. The UK-DMS500 particle emission meter was selected to measure PM particle size distribution and PM emission quality. The high-speed YOKOGAWA ScopeCorde was used to record the cylinder pressure from the Kistler 6117B piezoelectric high-pressure transducer (range: 0–20 MPa & sensitivity: −16.8 pc/bar). Corresponding crankshaft positions were measured by a Kistler 2613B crank angle encoder (sensitivity: 0.1–6°) with a resolution of 1 °CA. KSM-400 vertical static mixer was selected as the natural gas and hydrogen mixing device. The flow rates of CNG and H_2 were measured by a micro-motion flow meter (range: 0–40 kg/h (H2), 0–150 kg/h (CNG), sensitivity: ±0.2%) which used the principle of Coriolis force to directly measure mass flow. The target hydrogen fraction was obtained by adjusting the flow of CNG according to the flow of hydrogen through ALICAT flow control valve (sensitivity: ±0.4%). The main control software of the system was run based on Windows7 operating system and was developed using the virtual instrument development platform LabVIEW of NI. The engine specifications are shown in Table 1.

Numerical modeling and validation

The simulation in this work was conducted by the CONVERGE (Version 2.4) software. The premixed combustion mode is adopted in this simulation with the assumption of fully mixing in the spark ignition engine. *G* equation model was selected based on the flamelet theory of premixed turbulent combustion. In this method, turbulent flame front can be tracked by solving the Favre-averaged mean value of non-
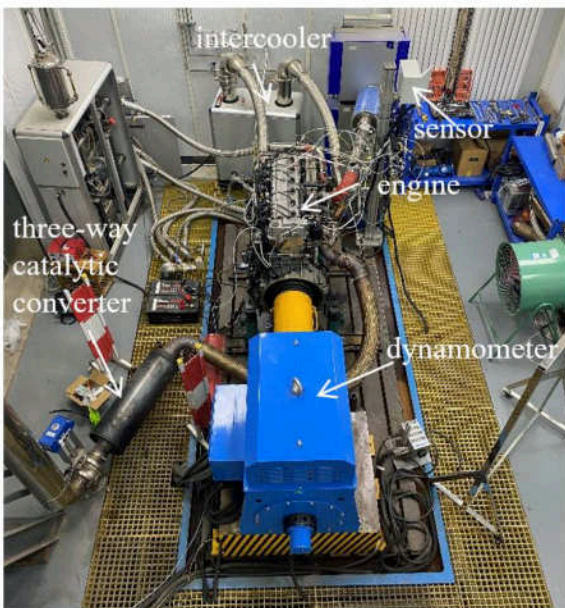

Fig. 1. Engine test platform in the current study.

Table 1
Engine specifications.

Engine parameters	Value
Bore/stroke (mm)	123/154
Connecting rod length (mm)	242.2
Combustion chamber structure	K11N
Compression ratio	11.51
Intake valve opening timing (°CA)	348.5
Exhaust valve opening timing (°CA)	129.5

reacting passive scalar *G* in corrugated flamelet or thin reaction zone regime [20].The transport equation of scalar *G* is shown by Eq. (1).

$$\frac{\partial \rho \widetilde{G}}{\partial t} + \frac{\partial \rho \widetilde{u}_i \widetilde{G}}{\partial x_i} = -D_t \kappa \left| \frac{\partial \widetilde{G}}{\partial x_i} \right| + \rho_u s_t \left| \frac{\partial \widetilde{G}}{\partial x_i} \right| \tag{1}$$

In above equation, s_t is the turbulent flame speed, ρ_u is the unburned gas density, D_t is the turbulent diffusion term, and κ is the mean flame front curvature. *G* is a passive scalar with $G = 0$ representing the flame surface where the chemical reaction happens. $G > 0$ ($G < 0$) represents the burned zone (unburned zone). The turbulent flame speed s_t is calculated by Eq. (2) .

$$s_t = s_l + u' \left\{ -\frac{a_4 b_3^2}{2b_1} D_a + \left[\left(-\frac{a_4 b_3^2}{2b_1} D_a \right)^2 + a_4 b_3^2 D_a \right]^{\frac{1}{2}} \right\} \tag{2}$$

where, u' is the turbulence speed fluctuation, s_l is the laminar flame speed, D_a is the Damköhler number, and a_4, b_1, b_3 are the model constants. In general, the laminar flame speed in Eq. (2) is usually input by the empirical formulas proposed by Gülder, Metghalchi et al. [21,22]. However, they are only applicable to a few fuels, such as isooctane, ethanol, methanol and their mixtures within limited operating conditions. The engine studied in this paper is a large-bore, low-speed, high-torque turbocharged natural gas engine. The thermodynamic conditions in the cylinder are beyond the consideration of these empirical formulas. Moreover, the influence of hydrogen addition on combustion and knocking is also considered in this paper. Therefore, based on the theory of Tabulated Laminar Flame-speed (TLF) [23], this paper uses a more general way to input laminar flame speed which was obtained by CONVERGE 1-D laminar flame solver [24] with the chemical mechanism of GRI3.0 [25], which is composed of 53 species and 325 reactions. Since the laminar flame speed depends on pressure, temperature, equivalence ratio and EGR, these parameters have to be considered when building the s_l table. The range and step length of each parameter are shown in Table 2. In the simulation, we used CH_4 instead of CNG. And the volume fraction of CH_4 accounts for 98% of CNG in the experiment.

To verify the accuracy of the laminar flame speed from the TLF table, we compared the laminar flame speed calculated by Chemkin and Converge under 0% H2 and 20% H2 conditions. Figure 2 provides the laminar flame speed calculated by two methods. The laminar flame speed calculated by the two methods is basically consistent. Therefore, the results calculated by Converge can be used as subsequent simulation calculations.

The visualization process of combustion in the cylinder shows that the occurrence of knocking is the spontaneous combustion of a part of the end mixture before the flame front of normal propagation reaches. In

Table 2
Parameter range of TLF.

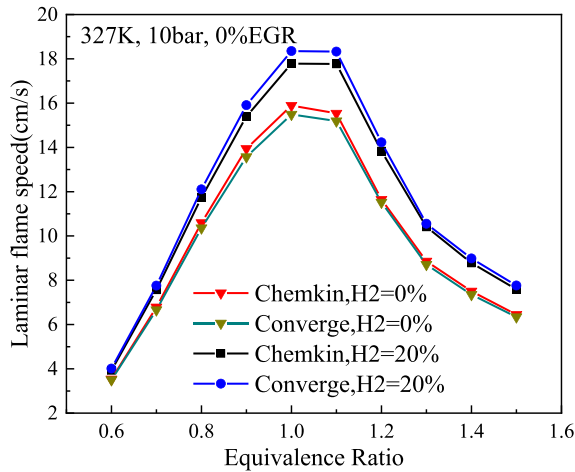| Parameter	Range	Step
Pressure (bar)	10–150	2
Temperature (K)	400–1200	50
Equivalence ratio	1.0	–
EGR	13.2218%	–

Fig. 2. The laminar flame speed calculated by Chemkin and Converge.

order to achieve knocking in the simulation, it is necessary to ensure that the mixture spontaneous combustion phenomenon can be captured in the unburned zone. The detailed chemical kinetic model is used outside the flame front [26]. Figure 3 depicts a schematic of the current combustion model. CEQ chemical balance solver was used to track the flame front and burned zone, and SAGE detailed chemical solver was used outside the flame (unburned zone). In addition, the multi-zone method is applied to further improve the computational efficiency. For details of this modeling method, the readers can refer reference [27].

The simulation calculation starts before the inlet valve opens and ends when the exhaust valve closes. A complete engine cycle is calculated. The corresponding 3D CAE model is obtained by extracting the physical model, as shown in Fig. 4. In this study, the basic grid size is 4 mm, and the cylinder grid is densified to 1 mm. Considering the accuracy of the intake manifold calculation, the grid is densified at the cone angle of intake valve. Two spherical densified areas with a radius of 2 mm and a radius of 4 mm are respectively set near the spark plug to accurately capture the spark core and the initial flame development. Due to the rapid changes in temperature and velocity during the combustion process, adaptive mesh refinement (AMR) is adopted to ensure the accuracy of combustion simulation. The maximum number of grids in the calculation process is about 2.4 million. The relevant grid parameters are shown in Table 3. The main models used in the simulation are shown in Table 4. The renormalization group RNG $k-\varepsilon$ model based on RANS with wall function is used to model the in-cylinder turbulence. RNG $k-\varepsilon$ model is widely used in engine modeling, which explains the key physical effects of flame propagation under engine conditions, such as compressibility effect. The second order central difference scheme is used for space discretization, and the first order implicit scheme is used for time discretization.
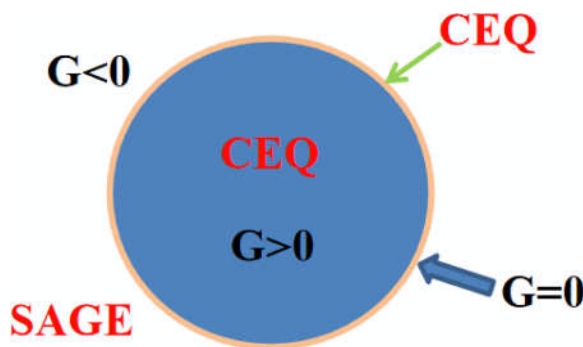

Fig. 3. Combustion model used in the burned zone and unburned zone.
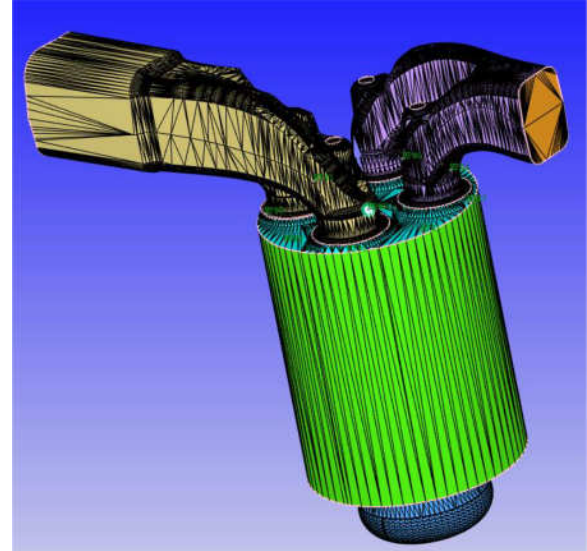

Fig. 4. Three-dimensional computational geometry model.

Table 3
Mesh parameter setting.

Mesh parameters	Value
Basic mesh	4 mm
Mesh at spark-plug	0.125–0.25 mm
Mesh at the cone angle of intake valve	0.5 mm
Mesh of cylinder	1 mm
Maximum number of meshes	2,400,000

Table 4
The models used in this study.

Turbulence model	RNG $k-\varepsilon$ model
Combustion model	G-equation coupled with GRI3.0 methane mechanism
Heat transfer model	O'Rourke and Amsden

The numerical simulation is based on a turbocharged four-stroke stoichiometric natural gas engine. The verification was carried out at 1000 rpm and 1963.4 N m. A grid dependency verification was firstly carried out for the established numerical models, and the test results are
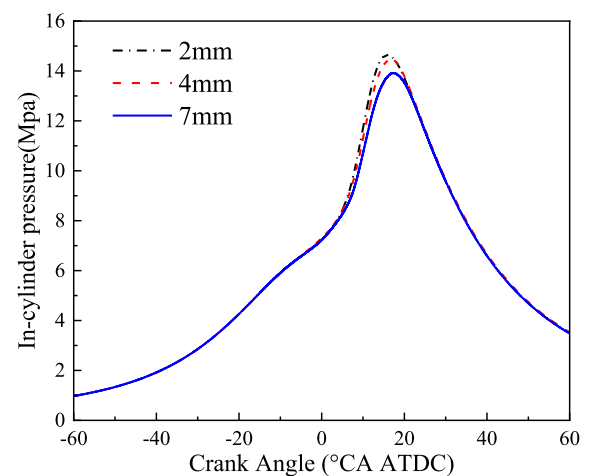

Fig. 5. Grid dependency verification: in-cylinder pressure predicted with different grid sizes (2 mm, 4 mm, and 7 mm).

shown in Fig. 5. It is clearly seen that a coarser grid size of 7 mm predicts a lower in-cylinder pressure, while the grid sizes of 4 mm and 2 mm predict the similar results. These variations may be due to the truncation error in solving second-order differential equations. Based on the simulation results, the grid size of 4 mm was selected for all the subsequent numerical simulations.

The specific simulation boundary conditions are shown in Table 5. The accuracy of the numerical simulation is verified by comparing the experimental and simulation results of the cylinder pressure and heat release rate curves. The validation method similar to the literatures [28, 29] is used here. The detailed verification results are shown in Fig. 6. It can be observed that the simulated curve is in the cyclic variation envelope of the experiment. However, there are some deviations between the experimental and simulation results. Firstly, there is uncertainty in the experiment, resulting in significant deviation in the pressure curves corresponding to different cylinders. At the same time, the model simplifies the combustion chamber structures, resulting in certain differences between the simulated and experimental structures. Therefore, the simulation cannot be completely consistent with the experimental results, but the current results satisfy the requirements of engine simulation and can be used for subsequent optimization work.

Knocking evaluation criteria

In this study, the cylinder pressure oscillation is used to identify the occurrence of knocking [29]. With the increase of knocking intensity (KI), the pressure oscillation amplitude should also increase [30]. Therefore, we use the maximum amplitude of pressure oscillation to evaluate knocking [28]. In the simulation, several numerical sensors are set at different positions of the combustion chamber to capture the pressure oscillation, as shown in Fig. 7. The collected pressure signal is filtered by band-pass filter (5–20 kHz) to obtain the maximum peak value of pressure oscillation which is designated as PPmax. The knocking intensity index KI is defined as the arithmetic mean value of PPmax at these different positions, which is shown in Eq. (3).

$$KI = \frac{1}{N}\sum_{n=1}^{N} PP_{\max,n} \tag{3}$$

Results and discussions

Experimental knocking

In order to obtain experimental data on knocking, we conducted HCNG engine tests based on the above experimental platform. The effects of different hydrogen ratios (20%, 40%) and different EGR rates on combustion characteristics were studied at 1100 rpm and medium to high loads (50%, 70%). During the experiment, we monitored the engine's knocking through the Kpeak value. The higher the Kpeak value, the greater the likelihood of knocking occurring. We generally believe that when the Kpeak value exceeds 1.5 in most cycles, the engine is in knocking operation. Considering the engine and related safety issues, the experiment only approached the knocking boundary and did not detect complete knocking.

Figure 8(a) shows the mean Kpeak values for different hydrogen ratios at different spark timings. The Kpeak value here is defined as the mean Kpeak value of the engine over 250 cycles. From the graph, we can
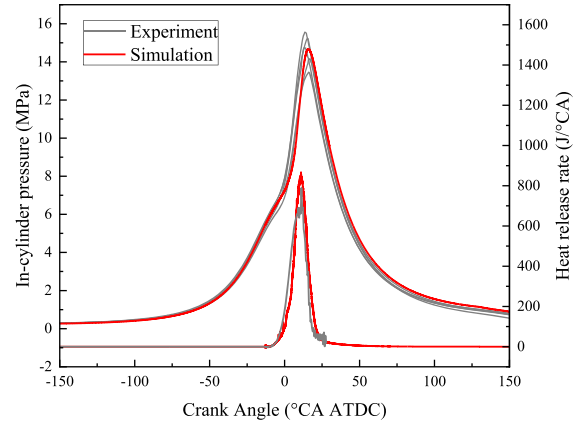

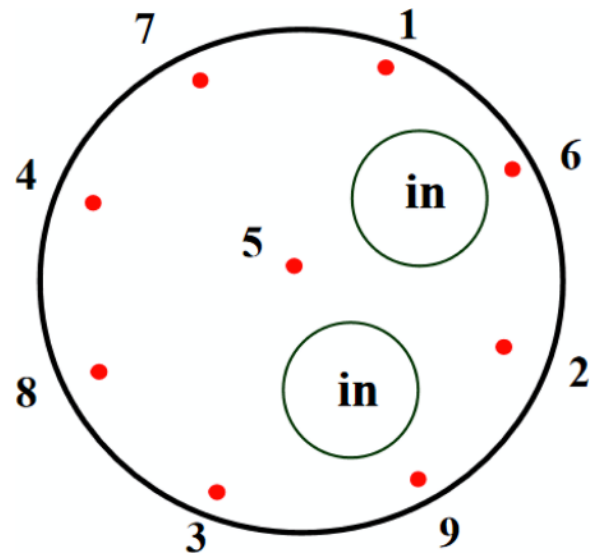**Fig. 6.** Model validation of in-cylinder pressure and heat release rate.

Fig. 7. Location of the numerical sensor in the combustion chamber.

observe that under the same spark timing conditions, with the increase of hydrogen ratio, the Kpeak value increases, which indicates an increasing trend of knocking. At the same time, as the spark timing advances, the Kpeak value also increases. The 40% hydrogen ratio shows a stronger upward trend. Figure 8(b) shows the effect of different hydrogen ratios and EGR rates on Kpeak value at 70% load operation. The effect of hydrogen addition is the same as the previous one, and as the load increases, the Kpeak value significantly increases. Under high load conditions, the spark timing is also delayed due to knocking limitation. Compared to pure natural gas, the maximum spark timing of the 20% hydrogen ratio condition is delayed by 9 °CA at 70% load operation. Figure 8(b) also shows the effect of EGR on knocking. As the EGR rate increases, the Kpeak value decreases. Therefore, knocking is suppressed, and the spark timing is also advanced.

To further demonstrate the experimental knocking phenomenon, we extracted the maximum Kpeak value cycle from 250 cycles for comparison. Under 50% load conditions, we selected the maximum spark timing of 40% hydrogen ratio as the benchmark, and the maximum Kpeak values corresponding to the three hydrogen ratios are 0.279 (0% H2), 0.604 (20% H2), and 2.918 (40% H2), respectively. Figure 9 shows the cylinder pressure curves corresponding to the maximum Kpeak value under different hydrogen ratios. It can be clearly observed from the figure that under the condition of 40% hydrogen ratio, the cylinder pressure has obvious sawtooth waves near TDC, and the peak value of

Table 5
Boundary conditions of simulation.

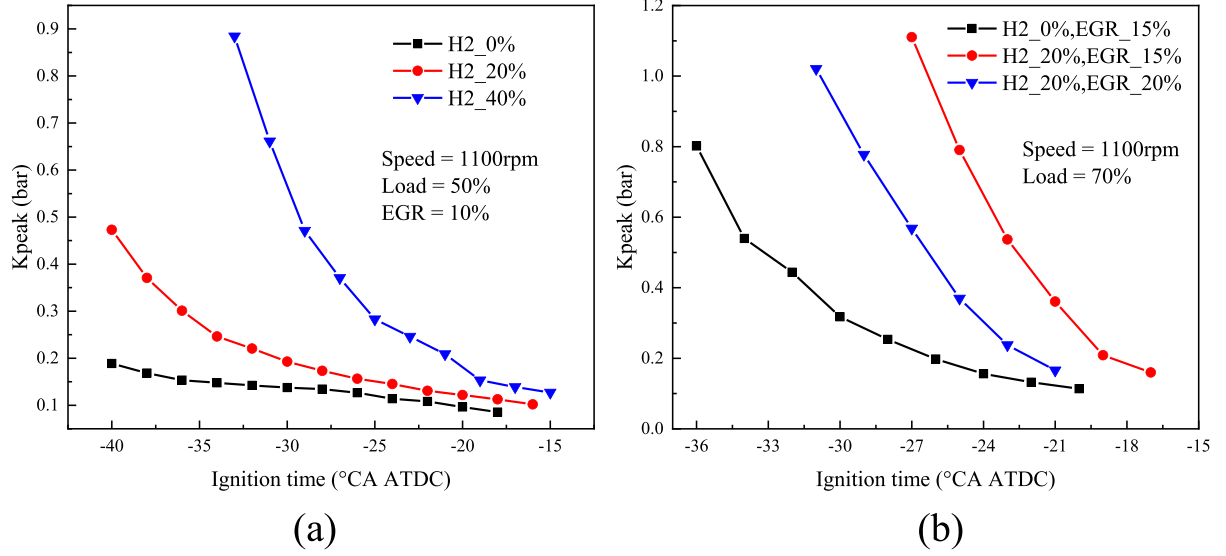| Boundary condition	Value
Speed/(r/min)	1000
EGR	13.2218%
Spark timing/ (°CA ATDC)	−13 °CA ATDC
Intake pressure/MPa	2.487
Intake temperature/K	327

Fig. 8. The mean Kpeak values for different hydrogen mixing ratios and EGR ratios at different spark timings. (a) 50%Load; (b) 70%Load.
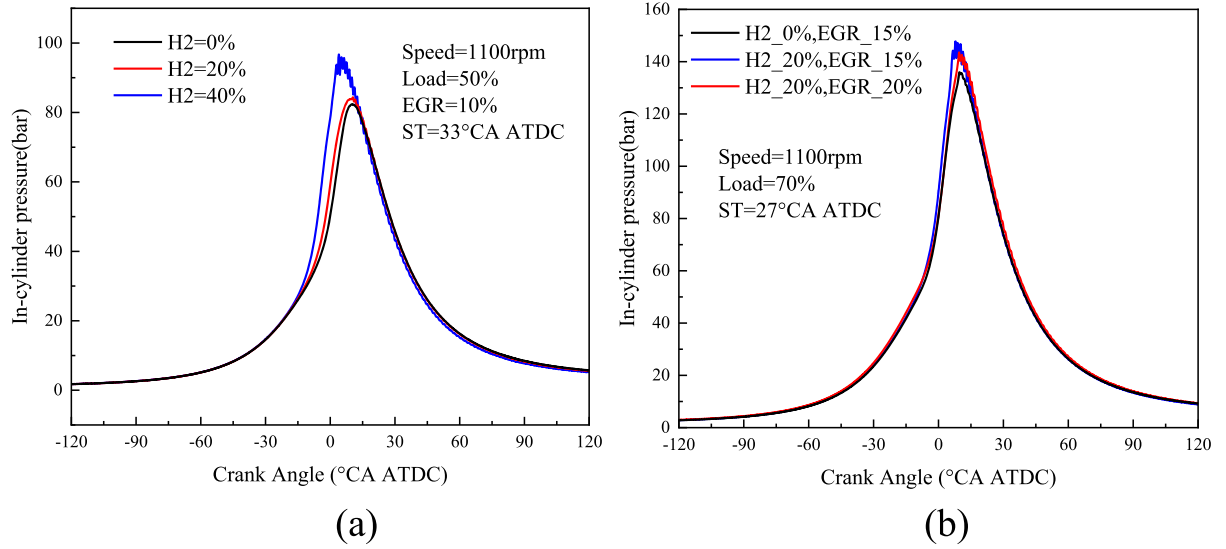

Fig. 9. The cylinder pressure corresponding to the maximum Kpeak value under different hydrogen mixing ratios.

cylinder pressure also increased significantly. Figure 9(b) shows the effects of different hydrogen ratios and EGR ratios on cylinder pressure under 70% load conditions. Similar to the previous results, the tendency to knocking increases with the increase of hydrogen. As the EGR rate increases, knocking is suppressed. At 70% load operation, the maximum Kpeak value corresponding to the 20% hydrogen ratio reaches 4.095.

Effect of combustion chamber geometry

The structure of the combustion chamber significantly affects the turbulence intensity of the engine. Higher turbulence intensity can achieve faster flame propagation, thus significantly suppressing knocking. Therefore, the optimization of combustion chamber has a great impact on engine performance. The chamber geometry of original engine is the reentrant shape, which is conducive to the formation of a squeeze flow to promote the mixing of fuel and air at the top dead center, but it is not easy to form a tumble flow, resulting in a low turbulence intensity in the combustion chamber.

The tumble ratio (TR) in *x* direction is defined as the ratio of the

angular speed of the flow about the center of mass in the *x* direction to the angular speed of the crankshaft, as shown in Eq. (4),

$$TR_x = \frac{\omega_1}{\omega_{crankshaft}} \tag{4}$$

where, ω_1 is the ratio of the angular speed of the flow about the center of mass in the *x* direction, $\omega_{crankshaft}$ is the angular speed of the crankshaft.

The swirl ratio (SR) is defined as the ratio of the angular speed of the flow about the center of mass in the *z* direction to the angular speed of the crankshaft, as shown in Eq. (5),

$$SR = \frac{\omega_2}{\omega_{crankshaft}} \tag{5}$$

where, ω_2 is the angular speed of the flow about the center of mass in the *z* direction, $\omega_{crankshaft}$ is the angular speed of the crankshaft.

Based on the above theory, under the condition of keeping a constant compression ratio, two piston geometries are designed for investigating the effect of combustion chambers on engine knocking and combustion.
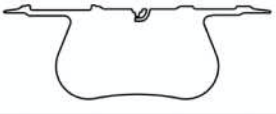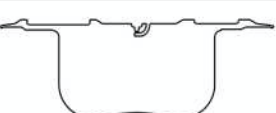
Chambers	chamber geometry
Case1: Reentrant	
Case2: Turbine	
Case3: Cylindrical	

Fig. 10. Three combustion chamber structures.

Figure 10 shows the comparison of the three chamber geometries used in this study.

Among the three cases, Case1 is the original combustion chamber structure of the engine. According to the experiment results, knocking occurs at the spark timing of −16 °CA ATDC. In the simulation, five spark timings of −13, −15, −16, −19, −22 °CA ATDC are calculated respectively. The pressure fluctuation at the monitoring point and the pressure oscillation curve after band-pass filtering are shown in Fig. 11

(a). As can be seen from the figure, with the advance of spark timing, the pressure at monitoring point 1 rises and the pressure oscillation increases. Figure 12(a) shows the KI value of Case1 at different spark timings. Based on the experimental results, knocking occurs at −16 °CA ATDC. It can be observed that the KI value of Case1 is maintained at about 0.06 MPa before the spark timing of −16 °CA ATDC. However, The KI value suddenly increases to 0.243 MPa at the spark timing of −16 °CA ATDC. Therefore, we believe that this model can accurately predict the experimental knocking conditions and 0.243 MPa can be used as the knocking threshold under this condition. It can also be seen from the diagram that further improvement of the spark timing can significantly increase the KI value. Figure 11(b) and (c) show the pressure fluctuations of Case2 and Case3 at monitoring point 1 and the pressure oscillation curves after band-pass filtering. It can be seen that the variation rules of Case2 and Case3 are basically the same as Case1.

Figure 12 shows the KI, IMEP and ITE of three Cases with different spark timings. We can observe that the KI values of Case2 and Case3 are lower than that of Case1, which indicates that the combustion chambers with cylindrical and turbine structure can significantly suppress knocking. According to the knocking threshold criterion set by Case1, knocking occurs at the spark timings of −19 °CA ATDC and −21 °CA ATDC for Case2 and Case3 with KI values of 0.27 MPa and 0.331 MPa respectively, which widens the knocking boundary. With the advance of spark timing, IMEP values of three cases show an increasing trend within the knocking boundary, especially for Case3. However, after the spark timing exceeds the knocking boundary, the IMEP of Case3 basically
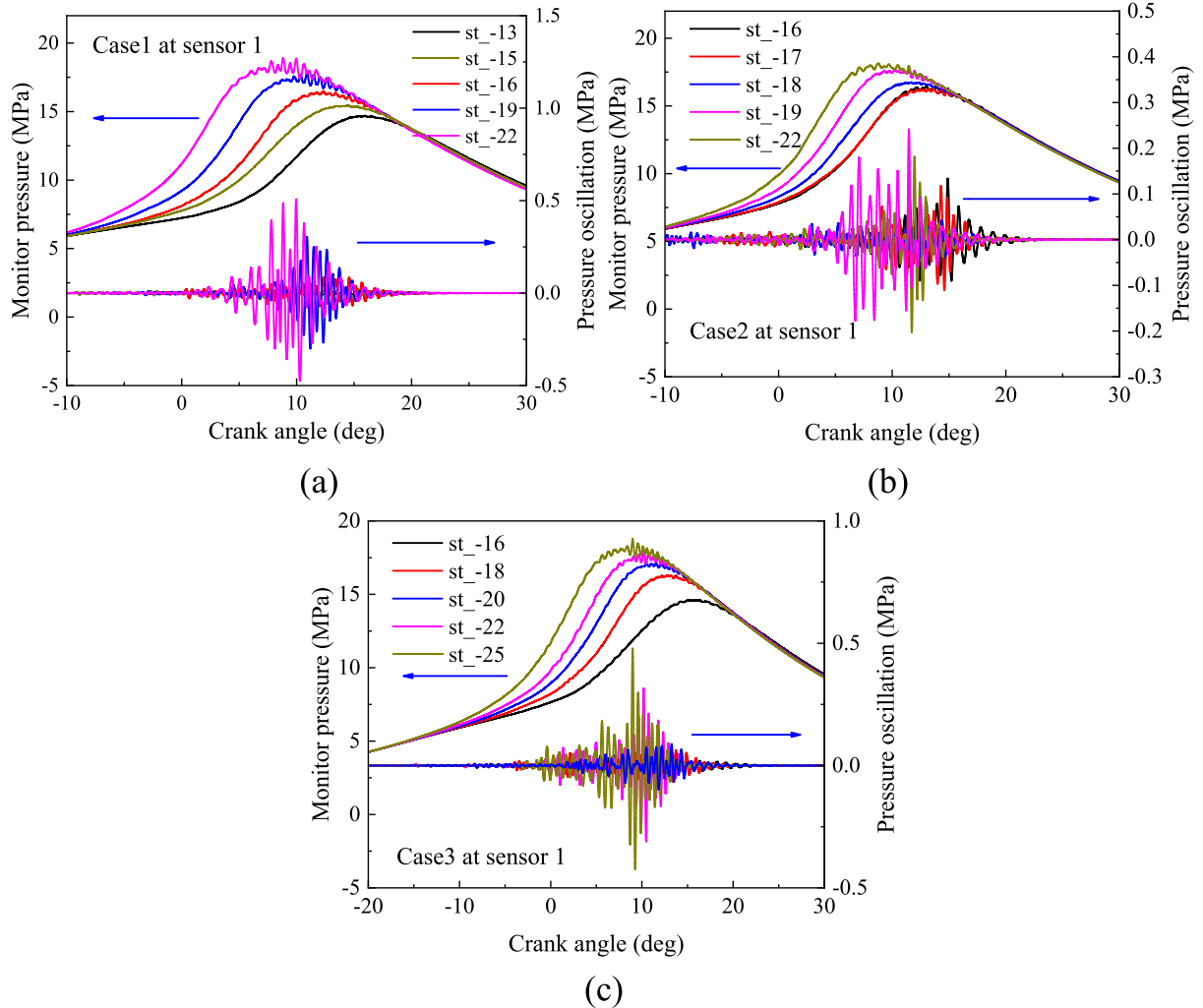

(a)

(b)

(c)

Fig. 11. Local pressure fluctuation and pressure oscillation after band pass filter for different chambers. (a) Case1; (b) Case2; (c) Case3.
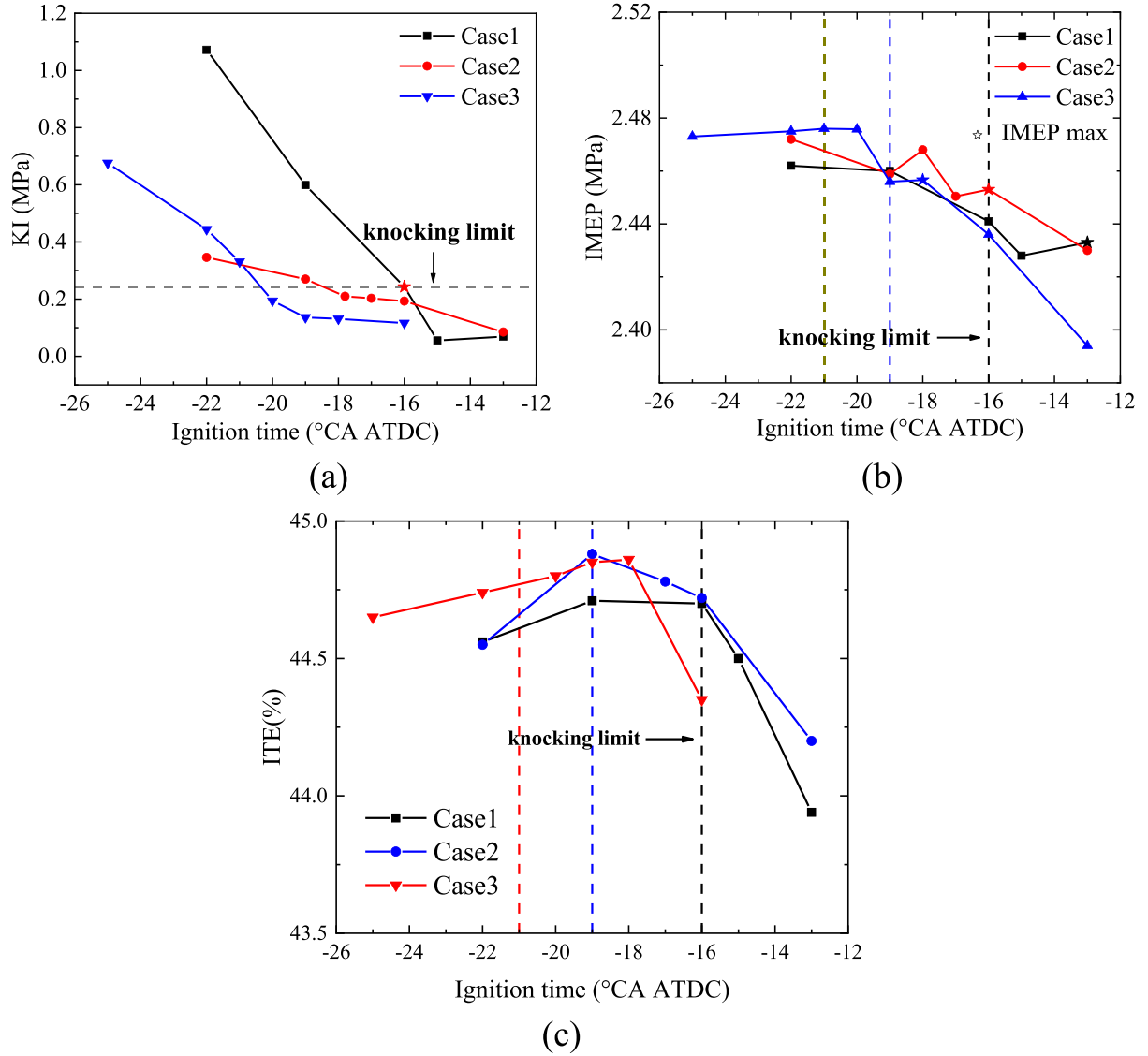
Fig. 12. (a) KI, (b) IMEP and (c) ITE of three cases at different spark timings.

reaches its peak value, which is mainly due to the increase of negative compression power. Considering the stability and reliability of the engine operation, the optimum spark timing is determined as the crankshaft rotation angle corresponding to 3 °CA ahead of the knocking occurrence time. Table 6 gives the IMEP values corresponding to optimum spark timings. It can be found in the table that the optimum IMEP values for Case2 and Case3 are higher than those for Case1 due to the extension of the knocking boundary. We can observe that as the spark timing advances, the indicated thermal efficiency first increases and then decreases. However, due to knocking limit, the spark timings of Case1 and Case2 cannot be located at the maximum ITE. Table 6 shows the optimum spark timing and corresponding IMEP and ITE of engine without knocking at different cases. Although Case2 is still subject to

knocking limit and cannot reach its maximum ITE, its optimal ITE under knocking limit is still higher than Case1. Meanwhile, the optimal spark timing for Case3 is located at the maximum ITE. The optimal ITE of Case2 and Case3 under knocking limit is higher than Case1, indicating that adjusting the combustion chamber structure can suppress engine knocking and improve the ITE.

To further analyze the impact of different chamber structures on knocking and combustion, Fig. 13 shows the curves of tumble, swirl and turbulent kinetic energy (TKE) with crankshaft angle. Both tumble and swirl flow will affect the turbulent intensity of the combustion chamber. From Fig. 13(a) and (b), it can be found that compared with the reentrant combustion chamber, the turbine and cylindrical shapes can increase the tumble flow to a certain extent. In addition, the swirl flow also increases. It is worth noting that although the cylindrical structure has a greater tumble ratio than the turbine structure, its tumble fragmentation during compression is worse than that of the turbine structure. In addition, the turbine structure has a relatively higher swirl ratio. Therefore, in Fig. 13(c), at the end of the compression stroke, the turbulence intensity of the turbine structure is significantly higher than the other two structures. Figure 14 shows the distribution of TKE of three cases at different crank angles. It can be seen that the overall TKE distribution of Case 2 is significantly higher than that of the other two

Table 6
Optimum spark timings and corresponding IMEP and ITE of engine without knocking at different cases.

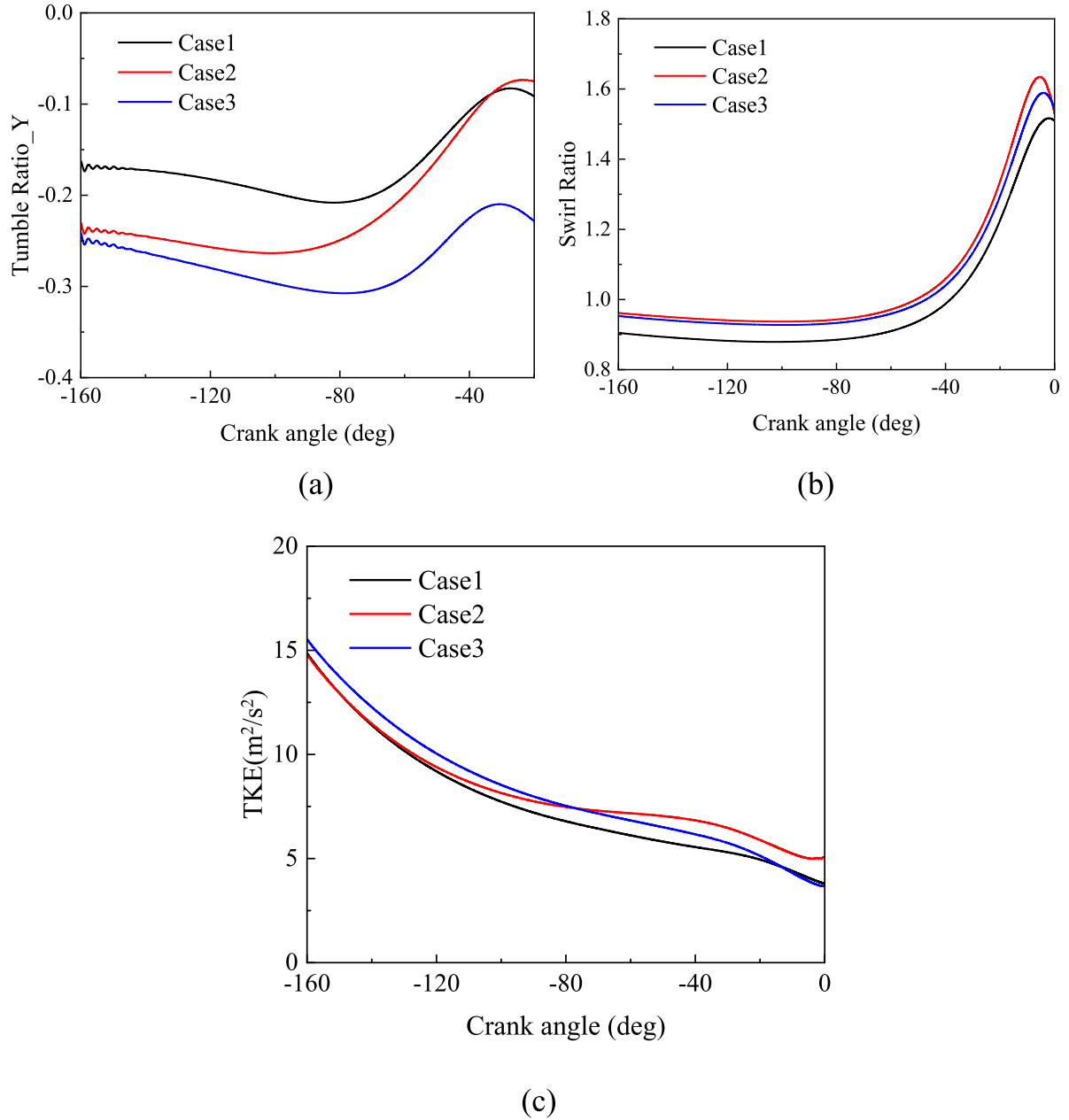| Chambers	Ignition time /°CA ATDC	IMEP/(MPa)	ITE (%)
Case1	−13	2.433	43.94
Case2	−16	2.453	44.72
Case3	−18	2.457	44.86

Fig. 13. In-cylinder (a) tumble, (b) swirl and (c) TKE of three cases at optimum spark timing.

Cases, which also verifies the TKE rule in Fig. 13(c). In addition, the TKE distribution of Case2 is closer to the inlet side, which is mainly caused by the air flow in the intake process. Figure 15 shows the G scalar distribution of three cases under different crankshaft angles. The G equation model tracks the flame surface propagation by solving the G scalar and $G = 0$ means it is on the flame surface. From the figure, we can see that at the initial stage of combustion, under the same spark timing, the flame propagation ranges of Case2 and Case3 are faster than that of Case1, which is mainly due to the wider knocking boundary leading to earlier spark timing. From the distribution of the flame surface, the flame propagation of the three cases is relatively uniform, but the flame propagation of the cylindrical structure is difficult near the lower wall of the combustion chamber due to the poor squish motion. Although the turbine structure also has the same problem, it is better than the cylindrical structure. Figure 16 shows the cylinder pressure, heat release rate and combustion phase of three cases under the optimal spark timing. Compared with Case1 and Case3, Case2 has the shortest combustion

duration in both CA10–50 and CA50–90, indicating that Case2 has better flame propagation. Besides, Case2 and Case3 achieve higher peak pressure and Case2 also has higher heat release rate. Therefore, based on the overall consideration consideration, Case2 is used as the subsequent knocking calculation.

Effect of hydrogen blending ratio

The combustion rate of hydrogen is fast. Mixing a small amount of hydrogen into natural gas can improve the combustion rate of natural gas and effectively reduce carbon emissions. Although hydrogen has a high-octane number, HCNG fuel is still subject to knocking due to the high combustion chamber temperature. Based on the above considerations, the effects of 10%, 20% and 30% hydrogen volume ratios on knocking and combustion are studied using the turbine structure determined in the previous article with constant intake pressure. It is worth mentioning that due to the change of combustion composition,
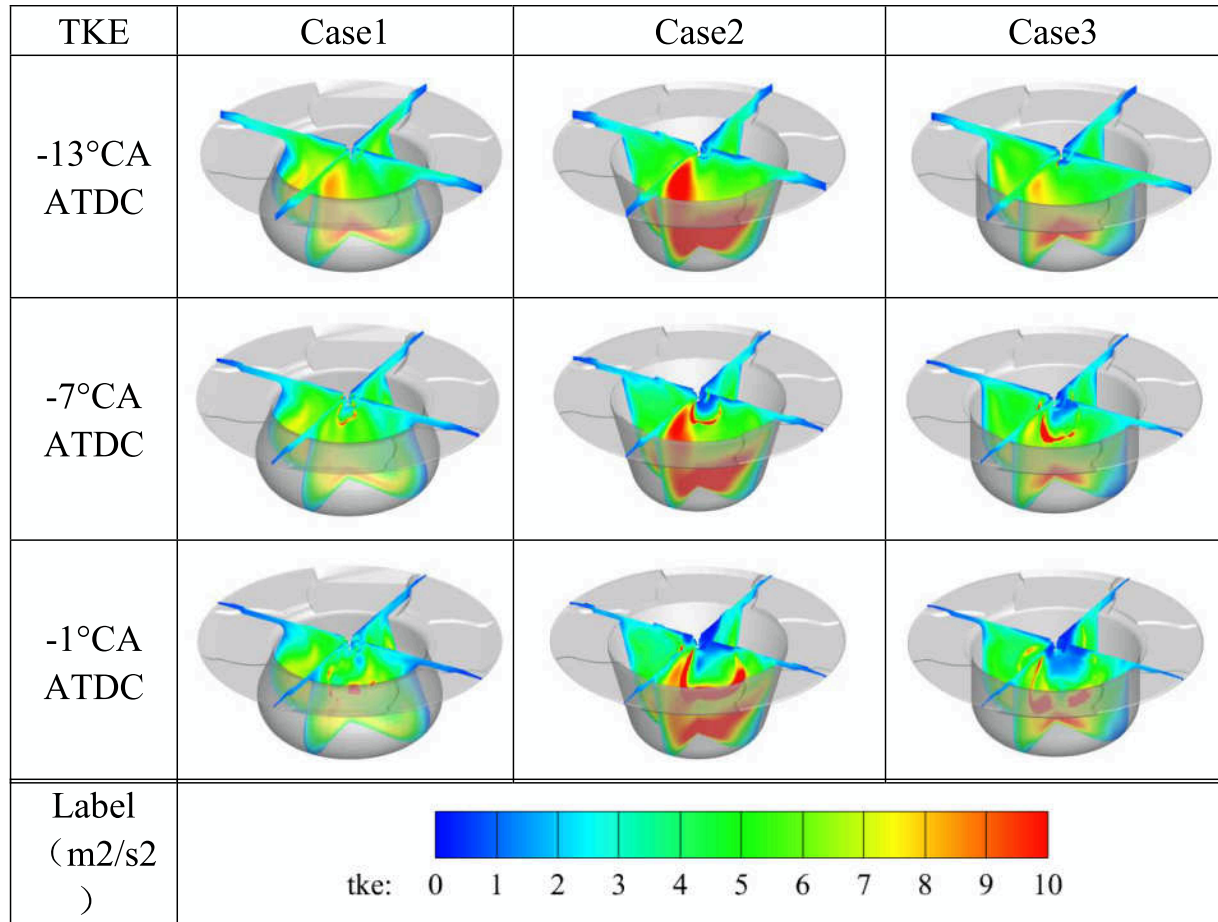
Fig. 14. Turbulent kinetic energy distribution of three cases at optimum spark timing with different crank angles.

each fuel mixture needs to redefine its TLF.

Figure 17 shows the KI, IMEP and ITE at different hydrogen ratios. It can be clearly observed from the figure that with the advance of the spark timing, the KI value of all mixed fuels will increase. The higher the mixing ratio of hydrogen, the more obvious the growth trend of its KI value. The KI value of 20% hydrogen volume ratio is basically the same as that of 10% hydrogen mixing near the knocking boundary, resulting in the same maximum spark timing of 10% and 20% hydrogen mixing. Table 7 shows the maximum spark timings and corresponding IMEP of the engine without knocking under different hydrogen ratios. The maximum spark timing is defined as the crankshaft rotation angle corresponding to 1 °CA ahead of the knocking occurrence time. Compared with pure natural gas, the maximum spark timings of all mixed fuels have been delayed, but with the increase of hydrogen ratio, the corresponding maximum spark timing has little change. In addition, since the inlet pressure remains unchanged and the volumetric heat value of hydrogen is lower than that of natural gas, the IMEP values of all mixed fuels will decrease under the addition of hydrogen. From the Fig. 17(c), it can be seen that with the advance of spark timing, when the spark timing is higher than −16 °CA ATDC, the ITE values of all mixed fuels are higher than that of pure natural gas. However, the maximum ITE of hydrogen mixing under knocking limit is lower than that of pure natural gas.

To clearly show the flame propagation process of the combustion chamber with different hydrogen ratios, the *G* scalar of different hydrogen ratios at different crankshaft angles is shown in Fig. 18. At the initial stage of combustion, with the increase of the hydrogen ratio, the flame propagation process gradually slows down under the same crankshaft angle condition. The 30% hydrogen mixing at −3 °CA ATDC

shows the slowest flame propagation. However, in the later stage of combustion, due to the faster combustion speed of hydrogen, the flame propagation of the four cases is basically similar. It is noteworthy that due to the defects of the turbine itself, the flame propagation on the lower wall of the combustion chamber is difficult. However, at the angle of the 17 °CA ATDC, the combustion condition of the lower wall of the combustion chamber has been improved with the increase of the hydrogen ratio and the flame covers the entire lower wall area of the combustion chamber.

Figure 19 shows the cylinder pressure, heat release rate and combustion phase at the maximum spark timing under different hydrogen ratios. It is basically the same as the previous conclusions that the spark timing is delayed due to the knocking limit, and the cylinder pressure after hydrogen addition is reduced greatly. Due to the faster combustion of hydrogen, the peak heat release rates of mixed fuels are higher than that of pure natural gas fuel, but the overall curves are relatively more right due to the late ignition. From the perspective of combustion phase, the conclusion also corresponds to the flame propagation image in the previous article. With the increase of hydrogen ratio, the duration of CA50–CA90 will be shortened, because the addition of hydrogen accelerates the combustion speed in the later stage of combustion. In general, simply increasing the mixing ratio of hydrogen will inhibit the knocking boundary of the engine. Although hydrogen mixing will improve the carbon emissions to a certain extent, delayed spark timing will inhibit the flame propagation and ultimately lead to the reduction of the engine's IMEP. Therefore, only changing the proportion of hydrogen cannot meet the operating requirements of the engine. EGR, as a technical measure, can effectively reduce the temperature of the combustion chamber, thus suppressing knocking. In order to study the effect of EGR
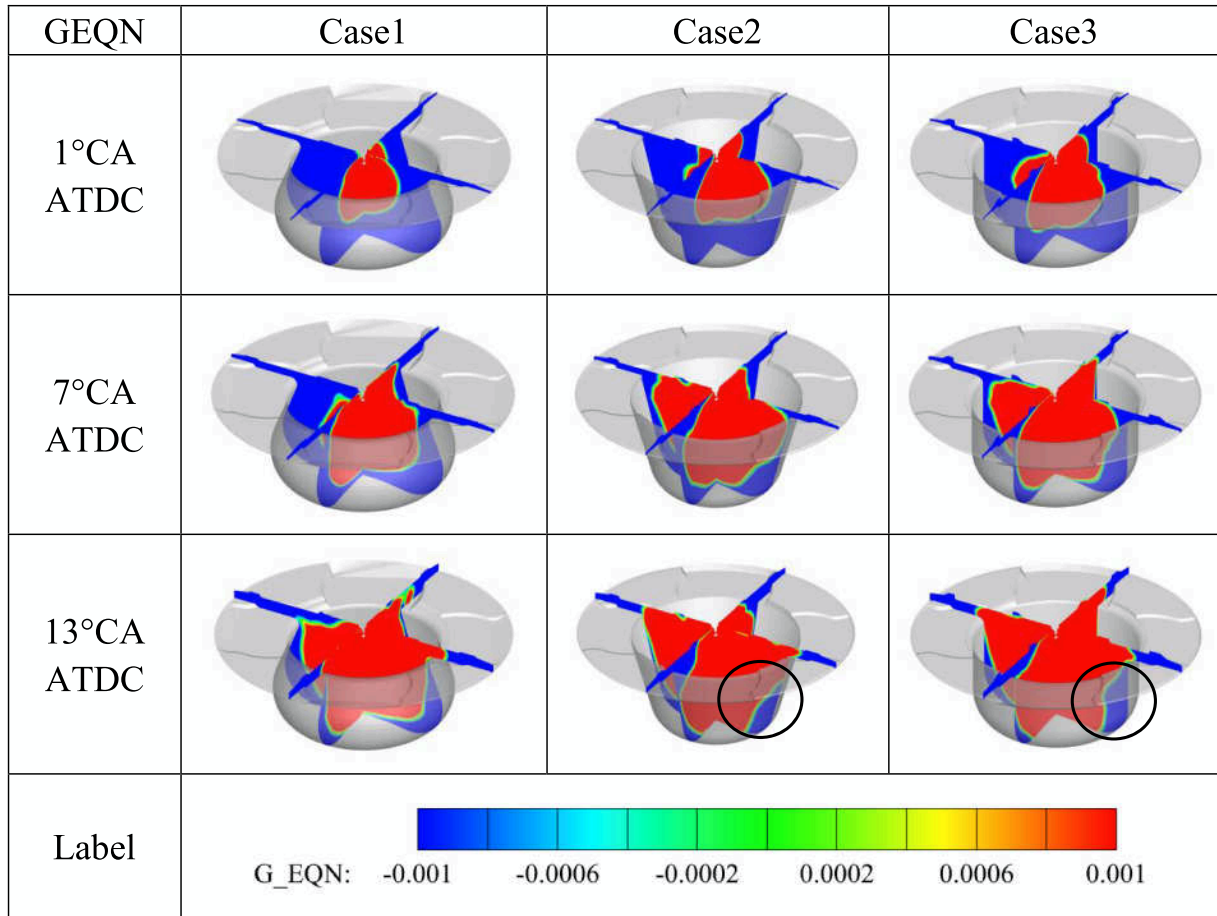
GEQN	Case1	Case2	Case3
1°CA ATDC			
7°CA ATDC			
13°CA ATDC			
Label	G_EQN: -0.001 -0.0006 -0.0002 0.0002 0.0006 0.001		

Fig. 15. *G* Scalar distribution of three Cases at optimum spark timing with different crankshaft angles.

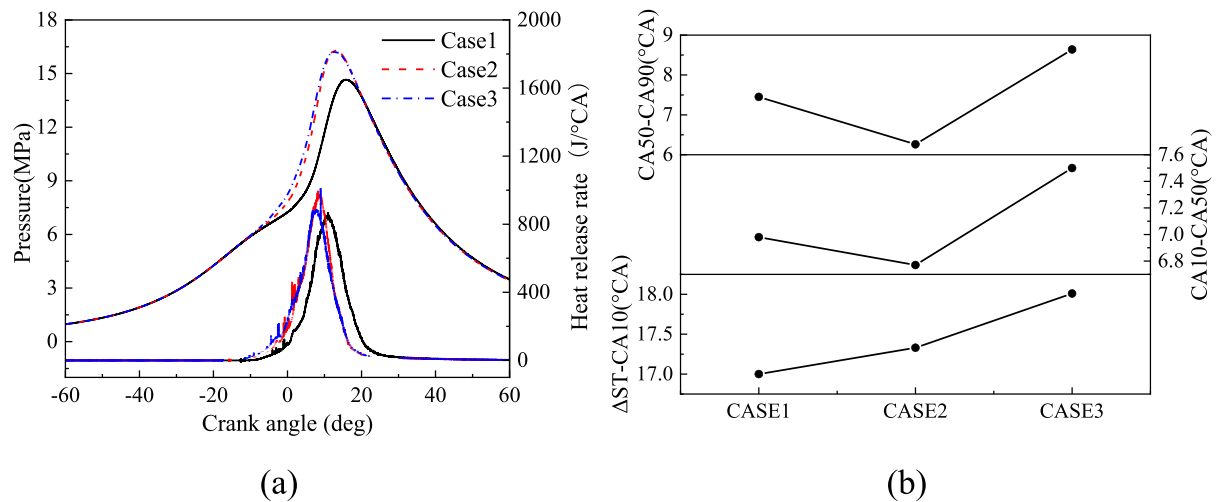(a)   (b)

Fig. 16. (a) In-cylinder pressure, heat release rate and (b) combustion phase of three cases at the optimum spark timing.

rate on knocking and combustion of HCNG engine, it is finally decided to use 30% HCNG fuel as the basis for subsequent research.

Effect of EGR rates

Based on the turbine structure and 30% hydrogen mixing, the effects of 14% (default), 20%, 25% and 30% EGR rates on engine knocking and combustion are studied. As before, since the adjustment of EGR rate will affect the laminar flame speed, we recalculated the TLF. Figure 20 shows the KI, IMEP and ITE at different EGR rates. From the figure, we can see that with the increase of EGR rate, the knocking tendency of the engine decreases gradually. In addition, no knocking was observed when the 30% EGR rate reached the peak of IMEP. Table 8 shows the maximum spark timings and corresponding IMEP and ITE of the engine without knocking at different EGR rates. Compared with the spark timing of 14% EGR rate, on this basis, 20% EGR rate is advanced by 5 °CA, 25% EGR
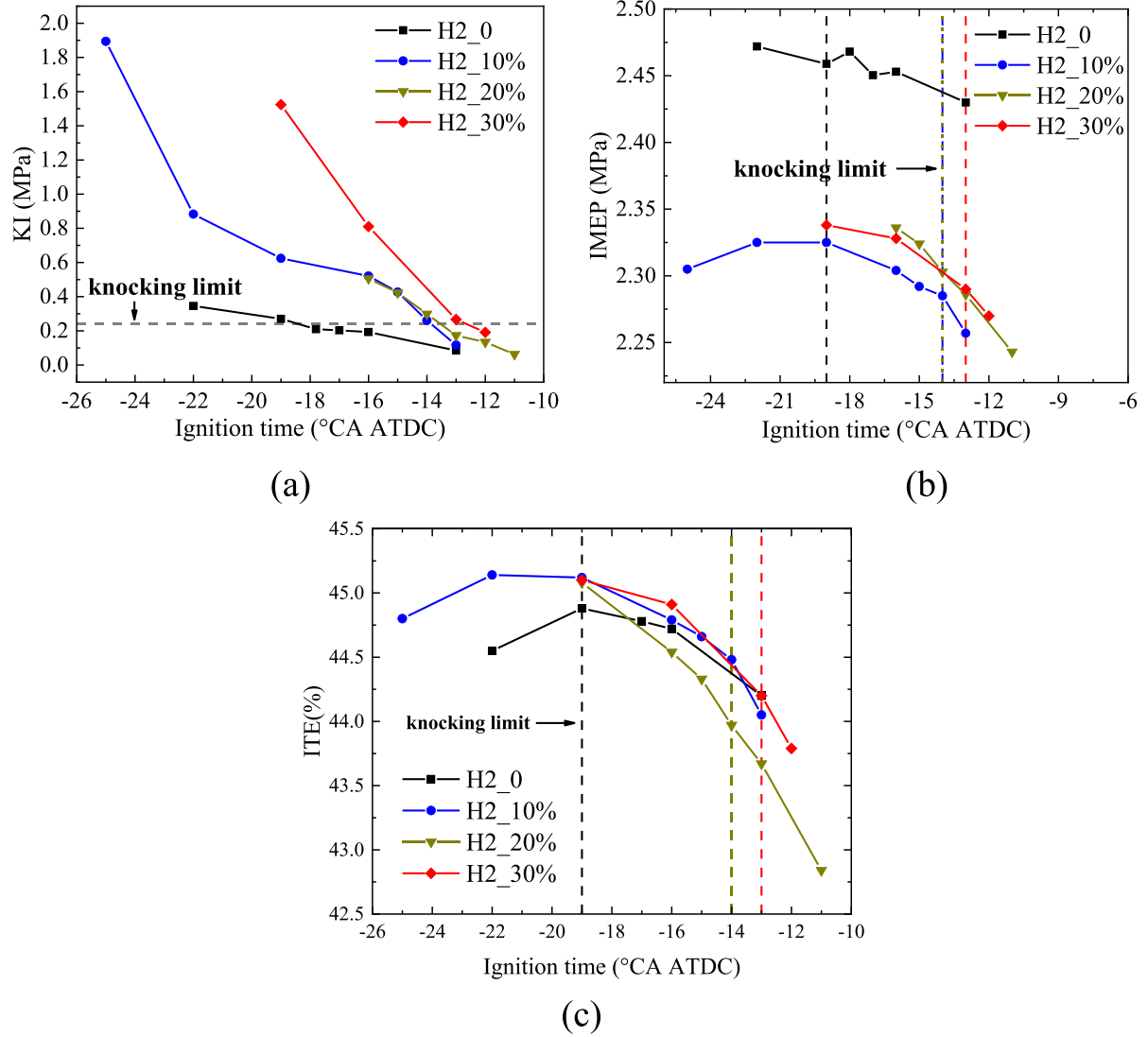
Fig. 17. (a) KI, (b) IMEP and (c) ITE at different hydrogen ratios.

Table 7
Maximum spark timings and corresponding IMEP and ITE of engine without knocking under different hydrogen ratios.

Hydrogen ratio	Ignition time /°CA ATDC	IMEP/(MPa)	ITE (%)
H2_0	−18	2.465	44.43
H2_10%	−13	2.257	44.05
H2_20%	−13	2.286	43.67
H2_30%	−12	2.27	43.79

the maximum spark timings corresponding to different EGR rates are shown in Table 8. Under the condition of maximum spark timing, the ITE increases with the increase of EGR rate. The ITE of 30% EGR rate reached 46.26%, which was 2.06% higher than that of 14% EGR rate.

Figure 21 shows the G scalar of different EGR rates at different crankshaft angles. It can be observed from the figure that at the initial stage of combustion, the flame propagation range increases with the increase of EGR rate. This is mainly due to the reduction of knocking tendency, thus achieving a more advanced spark timing. Fig. 22 shows the cylinder pressure, heat release rate and combustion phase of different EGR rates at the maximum spark timing. It can be seen from the figure that with the increase of EGR rate, the peak value of cylinder pressure decreases firstly and then increases and the cylinder pressure curve moves to the left as a whole. In addition, the peak heat release rate gradually decreases with the increase of EGR rate and the curve moves to the left as a whole. The increase of cylinder pressure is mainly due to the realization of a more advanced spark timing, while the decrease of the peak heat release rate is mainly due to the fact that the inlet pressure remains constant, which leads to the reduction of fuel. From the perspective of combustion phase, with the increase of EGR rate, the ignition delay and combustion duration will increase. This also shows the dilution effect of EGR rate.
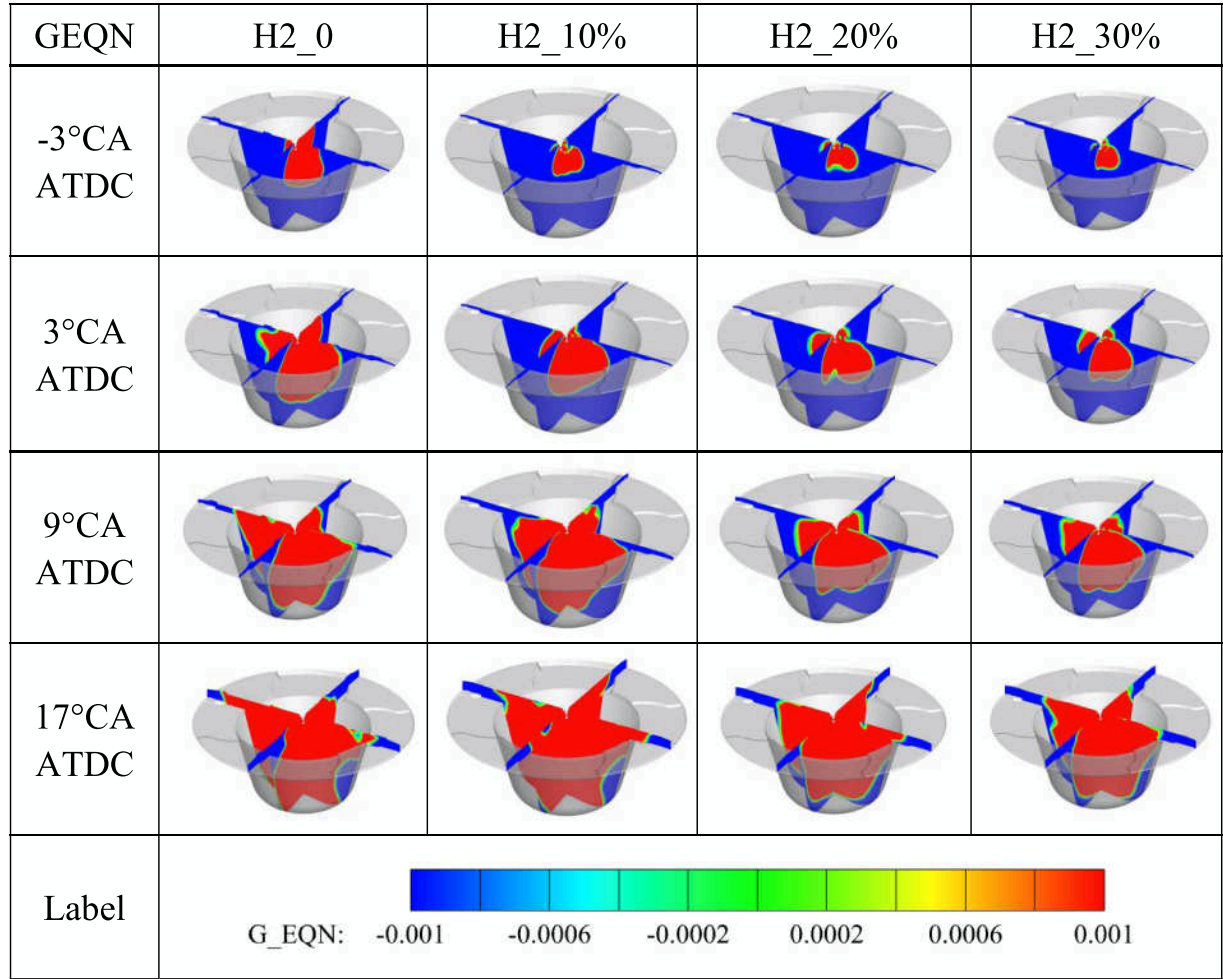
rate is advanced by 11 °CA and 30% EGR rate is advanced by 19 °CA. This shows that increasing EGR rate has a good ability to suppress knocking. Because of the high EGR rate, the temperature of the combustion chamber is reduced and the knocking suppression is realized. From the perspective of IMEP, with the increase of EGR rate, the engine's IMEP will decrease. This is mainly because under the condition that the inlet pressure remains constant, increasing the EGR rate will reduce the fuel and ultimately lead to the reduction of IMEP. With the continuous advance of the spark timing, the corresponding IMEP values increase under the four EGR rates and the improvement of IMEP is more obvious under the 20% EGR rate. As for the ITE, at the same spark timing, the ITE gradually decreases with the increase of EGR rate. However, due to the higher anti-knocking performance of high EGR rate,

Fig. 18. *G* reaction scalar at maximum spark timing with different hydrogen ratios and different crankshaft angle.
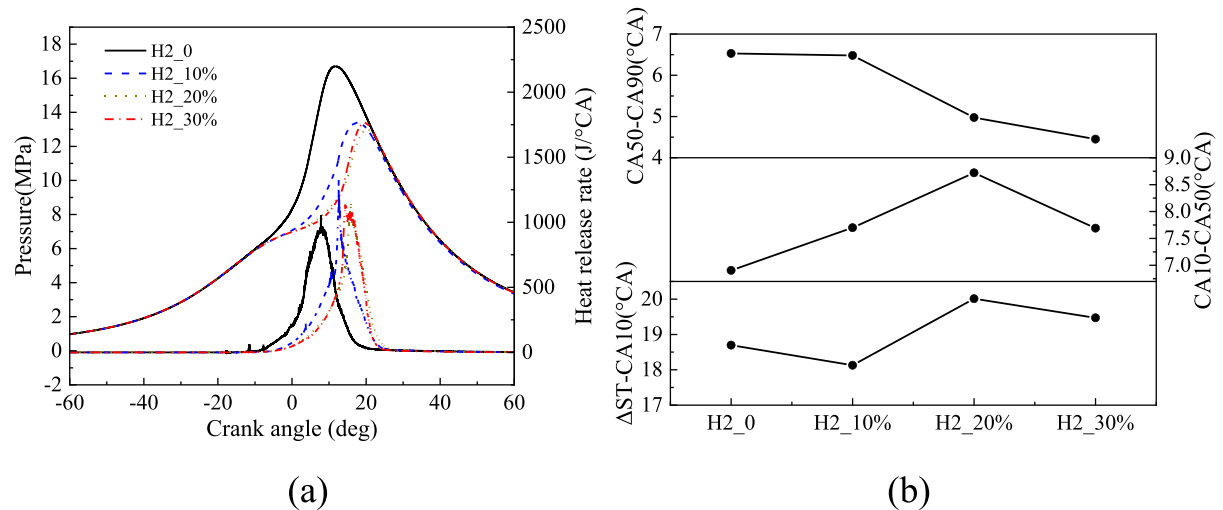

Fig. 19. (a) Cylinder pressure, heat release rate and (b) combustion phase at maximum spark timing with different hydrogen ratios.

Conclusions

In this work, the knocking and combustion characteristics of stoichiometric operation natural gas engine were studied by numerical simulation. The influence of different piston geometries on engine knocking and combustion was firstly investigated in this paper. In addition, the knocking and combustion characteristics under different hydrogen ratios and EGR ratios were also studied. The main conclusions are summarized as follows:
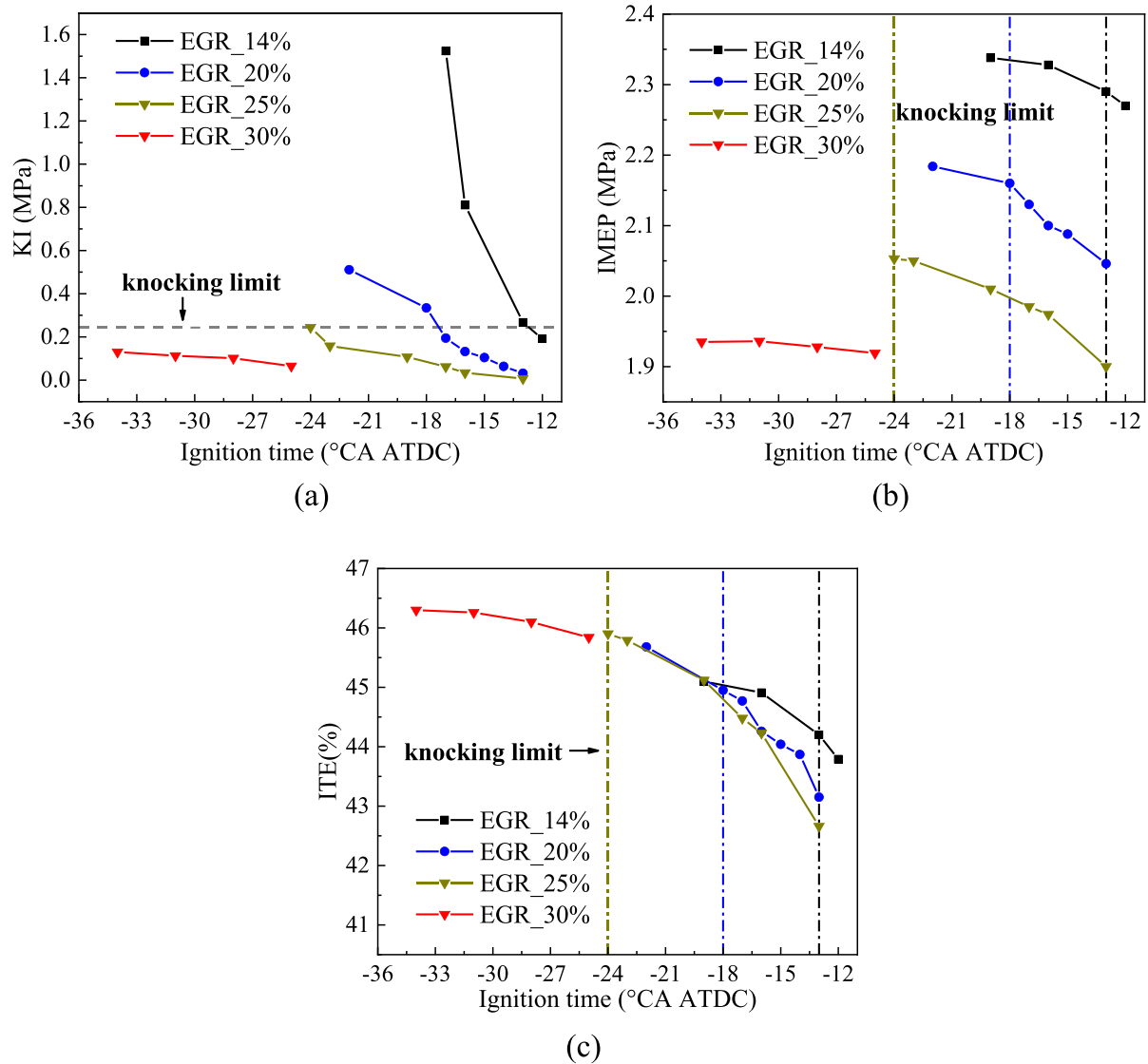
Fig. 20. (a) KI, (b) IMEP and (c) ITE at different EGR rates.

Table 8
Maximum spark timings and corresponding IMEP and ITE of engine without knocking at different EGR rates.

EGR	Ignition time /°CA ATDC	IMEP/(MPa)	ITE (%)
14%	−12	2.29	44.2
20%	−17	2.130	44.77
25%	−23	2.050	45.79
30%	−31	1.936	46.26

1 In the combustion model, the TLF method is used to input the laminar flame speed, which solves the calculation error of laminar flame speed caused by the empirical formula and achieves a higher thermodynamic and component range of laminar flame speed.

2 The effects of three different combustion chambers on knocking and combustion are studied. The turbulence intensity of the combustion chamber has a particularly critical impact on the knocking. Among the three combustion chamber structures, the turbine structure exhibits a higher swirl ratio and tumble crushing, resulting the highest turbulence intensity and the best anti-knocking performance. Compared with the reentrant structure, the spark timing of the turbine structure is advanced by 3 °CA, and the IMEP is increased by 0.2 bar.

3 The addition of hydrogen will increase the knocking tendency of the engine. Compared with pure natural gas, the maximum spark timing of 30% hydrogen mixing is delayed by 6 °CA. Due to the low volume heat value of hydrogen, the addition of hydrogen will also reduce the IMEP. However, the addition of hydrogen may accelerate the combustion rate at the end of combustion to a certain extent.

4 EGR can significantly reduce the knocking tendency of HCNG engine by reducing the combustion temperature in the cylinder. Compared with the case of 14% EGR rate, the spark timing of 30% EGR case is advanced by 19 °CA, and the indicated thermal efficiency is increased by 2.06%.

Declaration of Competing Interest

The authors declare that they have no known competing financial interests or personal relationships that could have appeared to influence the work reported in this paper.
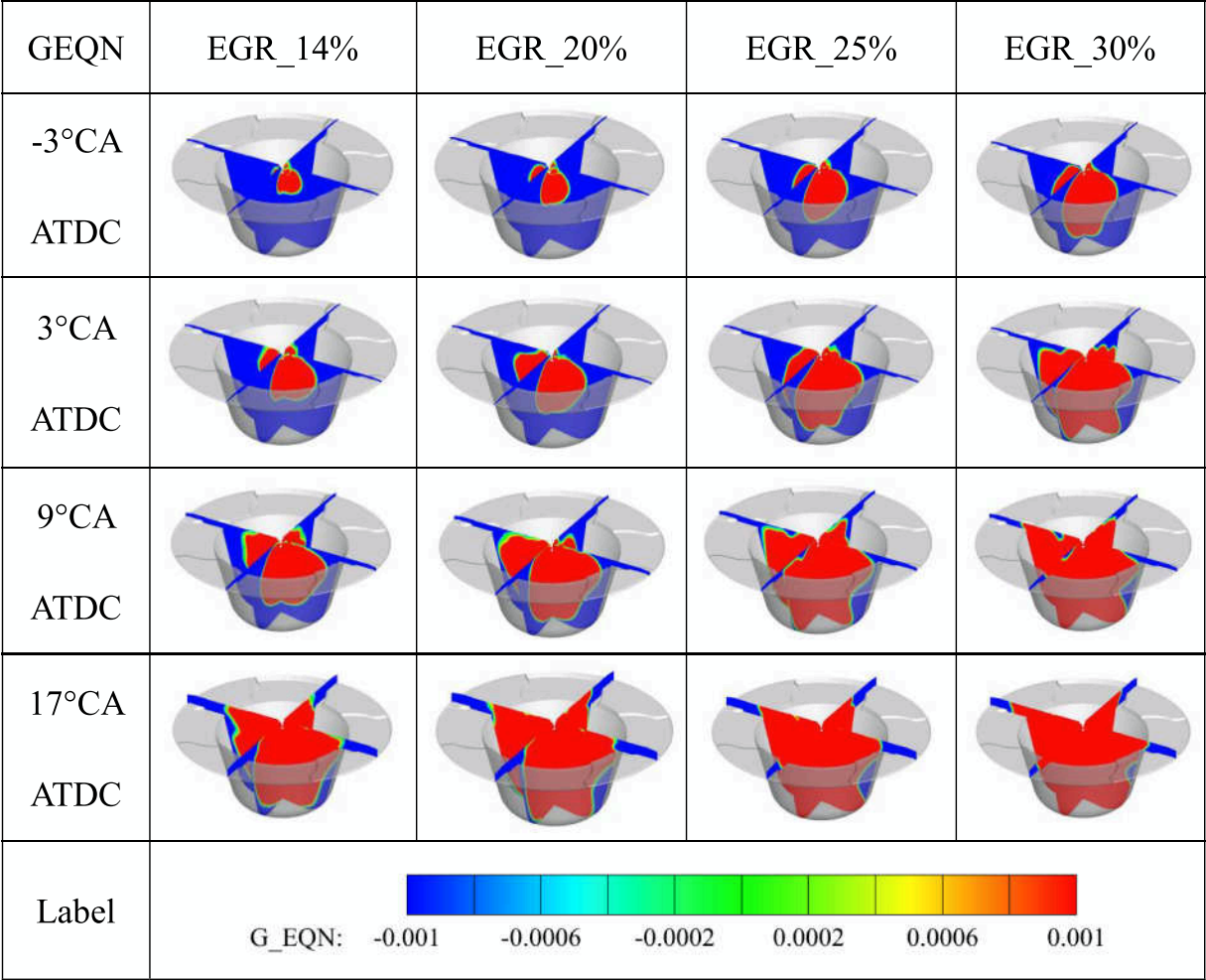
GEQN	EGR_14%	EGR_20%	EGR_25%	EGR_30%
-3°CA ATDC				
3°CA ATDC				
9°CA ATDC				
17°CA ATDC				
Label	G_EQN: -0.001 -0.0006 -0.0002 0.0002 0.0006 0.001			

Fig. 21. *G* scalar of different EGR rates at maximum spark timing with different crankshaft angles.
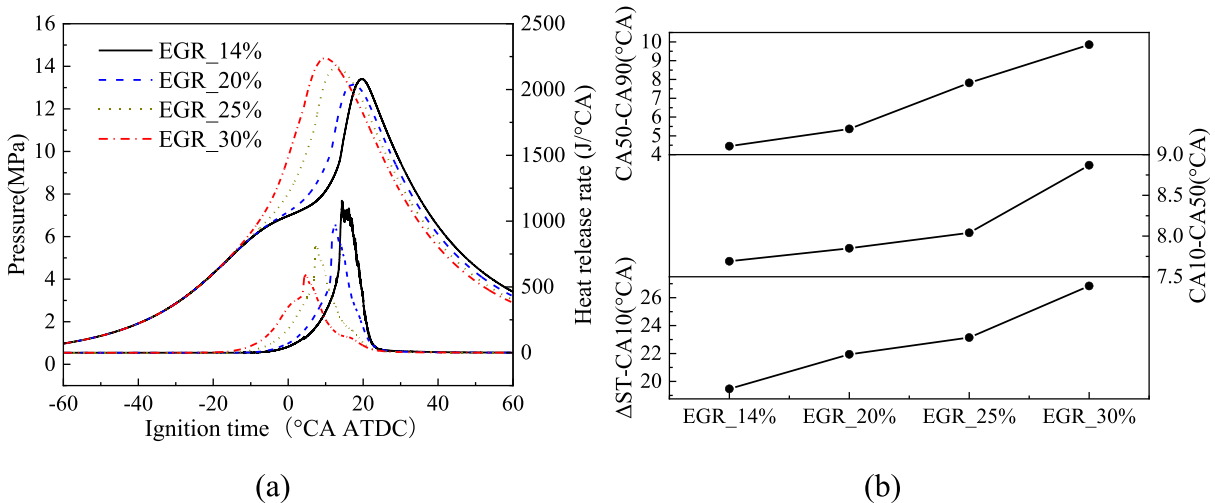

Fig. 22. (a) Cylinder pressure, heat release rate and (b) combustion phase of different EGR rates at maximum spark timing.

Data availability

No data was used for the research described in the article.

References

[1] Khan MI, Yasmin T, Shakoor A. Technical overview of compressed natural gas (CNG) as a transportation fuel. Renew Sustain Energy Revs 2015;51:785–97.

[2] Korakianitis T, Namasivayam AM, Crookes RJ. Natural-gas fueled spark-ignition (SI) and compression-ignition (CI) engine performance and emissions. Prog Energy Combust Sci 2011;37:89–112.

[3] Johansson B, Olsson K. Combustion chambers for natural gas SI engines part I: fluid flow and combustion. SAE International; 1995.

[4] Einewall P, Johansson B. Combustion chambers for supercharged natural gas engines. SAE International; 1997.

[5] Li F, Liu C, Song H, Wang Z. Improving combustion and emission characteristics in heavy-duty natural-gas engine by using pistons enhancing turbulence. SAE International; 2018.

[6] Gómez Montoya JP, Amell Arrieta AA. Effect of the turbulence intensity on knocking tendency in a SI engine with high compression ratio using biogas and blends with natural gas, propane and hydrogen. Int J Hydrogen Energy 2019;44: 18532–44.

[7] Yan B, Tong L, Wang H, Zheng Z, Qin Y, Yao M. Experimental and numerical investigation of the effects of combustion chamber reentrant level on combustion characteristics and thermal efficiency of stoichiometric operation natural gas engine with EGR. Appl Therm Eng 2017;123:1473–83.

[8] Zhao X, Wang H, Zheng Z, Yao M, Sheng L, Zhu Z. Evaluation of knock intensity and knock-limited thermal efficiency of different combustion chambers in stoichiometric operation LNG engine. SAE International; 2019.

[9] Zhu Z, Zhong X, Zhao X, Wang Y, Zheng Z, Yao M, Wang H. Numerical investigation on combustion system optimization of stoichiometric operation natural gas engine based on knocking boundary extension. Fuel 2021;290:120092.

[10] Ma F, Wang M, Jiang L, Deng J, Chen R, Naeve N, Zhao S. Performance and emission characteristics of a turbocharged spark-ignition hydrogen-enriched compressed natural gas engine under wide open throttle operating conditions. Int J Hydrogen Energy 2010;35:12502–9.

[11] Rao A, Wu Z, Kumar Mehra R, Duan H, Ma F. Effect of hydrogen addition on combustion, performance and emission of stoichiometric compressed natural gas fueled internal combustion engine along with exhaust gas recirculation at low, half and high load conditions. Fuel 2021;304:121358.

[12] Flekiewicz M, Kubica G, Flekiewicz B. Identification of optimal CNG -hydrogen enrichment ratio in the small SI engines. SAE International; 2012.

[13] Sagar SMV, Agarwal AK. Knocking behavior and emission characteristics of a port fuel injected hydrogen enriched compressed natural gas fueled spark ignition engine. Appl Therm Eng 2018;141:42–50.

[14] Yu C, Zhao Z, Wang L, Cui H, Zhang F. The effect of cooled EGR on combustion and load extension in a kerosene spark-ignition engine. Fuel 2020;280:118681.

[15] Zhen X, Wang Y, Xu S, Zhu Y. Numerical analysis on knock for a high compression ratio spark-ignition methanol engine. Fuel 2013;103:892–8.

[16] Li X, Zhen X, Wang Y, Liu D, Tian Z. The knock study of high compression ratio SI engine fueled with methanol in combination with different EGR rates. Fuel 2019; 257:116098.

[17] Wei H, Feng D, Pan J, Shao A, Pan M. Knock characteristics of SI engine fueled with *n*-butanol in combination with different EGR rate. Energy 2017;118:190–6.

[18] Zhen X, Tian Z, Wang Y, Xu M, Liu D, Li X. Knock analysis of bio-butanol in TISI engine based on chemical reaction kinetics. Energy 2022;239:122190.

[19] Kar T, Fosudo T, Marchese A, Windom B, Olsen D. Effect of fuel composition and EGR on spark-ignited engine combustion with LPG fueling: experimental and numerical investigation. Fuel 2022;327:125221.

[20] Kim SH. A front propagation formulation for under-resolved reaction fronts. J Comput Phys 2015;285:193–207.

[21] Ryan TW, Lestz SS. The laminar burning velocity of isooctane, *N*-heptane, methanol, methane, and propane at elevated temperature and pressures in the presence of a diluent. SAE International; 1980.

[22] Gülder ÖL. Correlations of laminar combustion data for alternative S.I. engine fuels. SAE International; 1984.

[23] Silva M, Liu X, Hlaing P, Sanal S, Cenker E, Chang J, Johansson B, Im HG. Computational assessment of effects of throat diameter on combustion and turbulence characteristics in a pre-chamber engine. Appl Therm Eng 2022;212: 118595.

[24] Pal P, Kolodziej CP, Choi S, Som S, Broatch A, Gomez-Soriano J, Wu Y, Lu T, See YC. Development of a virtual CFR engine model for knocking combustion analysis. SAE Int J Engines 2018;11:1069–82.

[25] G.P. Smith, D.M. Golden, Michael Frenklach N.W., Moriarty B.E., MikhailGoldenberg, C., Thomas Bowman R.K., Hanson S.S., William C., et al. GRI-Mech 3.0;1999. Available from: http://www.me.berkeley.edu/gri_mech/.

[26] Iyer CO, Yi J, Liang L, Reitz RD. Modeling knock in spark-ignition engines using a G-equation combustion model incorporating detailed chemical kinetics. SAE International; 2007.

[27] Draper CS. Pressure waves accompanying detonation in the internal combustion engine. J Aeronaut Sci 1938;5:219–26.

[28] Chen L, Pan J, Wei H, Zhou L, Hua J. Numerical analysis of knocking characteristics and heat release under different turbulence intensities in a gasoline engine. Appl Therm Eng 2019;159:113879.

[29] Zhao X, Zhu Z, Zheng Z, Yue Z, Wang H, Yao M. Effects of flame propagation speed on knocking and knock-limited combustion in a downsized spark ignition engine. Fuel 2021;293:120407.

[30] Robert A, Richard S, Colin O, Martinez L, De Francqueville L. LES prediction and analysis of knocking combustion in a spark ignition engine. Proc Combust Inst 2015;35:2941–8.